

## Article

# Insights into Phosphate Adsorption Performance onto Magnetic Thermal Modified Palygorskite Nanocomposites

Min Pan <sup>1</sup> , Jingfeng Su <sup>1</sup>, Leting Tang <sup>1</sup>, Zimin Hu <sup>1</sup> and Xiaoming Huang <sup>1,2,\*</sup> 

<sup>1</sup> Fujian Engineering and Research Center of Rural Sewage Treatment and Water Safety, School of Environmental Science and Engineering, Xiamen University of Technology, Xiamen 361024, China

<sup>2</sup> Key Laboratory of Water Resources Utilization and Protection of Xiamen, Xiamen University of Technology, Xiamen 361024, China

\* Correspondence: huangxm@xmut.edu.cn

**Abstract:** Eutrophication caused by excessive discharging of phosphorus is a global water pollution problem. To further improve the phosphorus adsorption capacity of natural palygorskite and easy separation from liquid, magnetic thermal modified palygorskite nanocomposite (MTPG) was firstly fabricated and then characterized by XRD and SEM-EDS. The characterization results showed Fe<sub>3</sub>O<sub>4</sub> in nano-diameters was prosperously immobilized on the surface of thermal modified palygorskite (TPG) calcinated at a temperature of 700 °C. Abundant nano-scale Fe<sub>3</sub>O<sub>4</sub> loading almost doubled the specific surface area (SSA) of TPG. The adsorption of phosphate onto MTPG was highly pH-dependent and slightly influenced by ionic strength. According to the results from the Langmuir model, the maximum adsorptive quantity of 400.00 mg/g was counted at 298 K. The regeneration ratio was 80.98% after three regeneration cycles. The process of phosphate adsorption was confirmed to be an endothermic and spontaneous chemisorption. Thus, the cost-effective, excellent phosphate affinity, great magnetic recovery performance, and high adsorption capacity of MTPG had an enormous promising utilization on phosphate removal from aqueous solutions.

**Keywords:** phosphorus; palygorskite; magnetic recovery; kinetics; thermodynamics



**Citation:** Pan, M.; Su, J.; Tang, L.; Hu, Z.; Huang, X. Insights into Phosphate Adsorption Performance onto Magnetic Thermal Modified Palygorskite Nanocomposites. *Minerals* **2023**, *13*, 293. <https://doi.org/10.3390/min13020293>

Academic Editors: Raúl Fernández, Gujie Qian, Yan Zhou and Weifeng Chen

Received: 24 January 2023

Revised: 10 February 2023

Accepted: 17 February 2023

Published: 20 February 2023



**Copyright:** © 2023 by the authors. Licensee MDPI, Basel, Switzerland. This article is an open access article distributed under the terms and conditions of the Creative Commons Attribution (CC BY) license (<https://creativecommons.org/licenses/by/4.0/>).

## 1. Introduction

Phosphorus is a crucial nutrient substance for growth of organisms on earth. Huge demand triggers excessive discharge of phosphorus from industrial (mainly detergents and cleaners) and agricultural systems, which causes eutrophication of water bodies and is harmful for aquatic plants. The World Health Organization (WHO) has established a maximum discharge criteria of 0.5–1.0 mg P/L for the receiving water body [1]. In practical engineering application, numerous developed treatment techniques have been verified to scavenge phosphorus from aquatic medium, including chemical method (mainly including precipitation and ion exchange), biological method, and adsorption [2–5]. Among those, the success of the biological treatment technique in phosphorus removal has been certificated for a long time. However, complex operation system (including aeration, non-aeration, and backflow), high operation cost, complex management, and large structure floor area limit its practical application. It was recommended for the treatment of wastewater containing 0.3–2 mg/L of phosphorus [6]. Additionally, the excess sludge containing phosphorus required further thickening and dehydration, otherwise, it will cause secondary pollution. Chemical method is widely applied for phosphorus removal, but the addition of metal salts causes heavy effluent color and large production of sludge [2]. Importantly, phosphorus is one type of non-renewable resource in the abundant natural resources [7–9]. Thus, the growing needs of phosphorus would be possibly overcome by recovering phosphate from wastewater, which become a global consensus [7]. The technology of adsorption attracts great attention on phosphate removal and recycling due to its convenient operation process, flexibility of design, low cost, and high effectiveness and reusability [3]. However,

the adsorption process highly relies on the properties of adsorbents. To accommodate wide concentration range of phosphate removal and achieve an ultralow level of effluent requirement, various adsorbents have been explored, such as minerals, biochars, red mud, metal (hydr)oxides, layered double hydroxide [3,7,10–13]. To find environmentally friendly, economic, high adsorptive capacity, and efficient adsorbents, great endeavors are still demanded.

Natural palygorskite (PG) is a typical nano-fibrous magnesium-aluminum hydrated phyllosilicate clay mineral, which abundantly exists in a natural environment [3,14]. It possesses a unique rod-like crystal structure (40 nm crystal diameter), a large specific surface, tunable surface chemistry, high dispersion, and well-developed nanopores, which make it a promising adsorbent [15]. As reported, raw PG and modified PG have been explored to adsorb phosphate, ammonium, fluoride ions, heavy metals (for example, arsenate,  $\text{Cu}^{2+}$ ,  $\text{Ag}^+$ ), methylene blue, and phenol [16–25]. However, raw PG has limited active sites, nonuniform distribution of intrinsic constituents, and limited surface area, which rigorously restricts the performance of phosphorus adsorption [23]. Thus, many efforts have been expended to magnify its adsorptive capacity by expanding the specific surface area (SSA) or multiplying the active sites. A typical modification method of thermal treatment has long been used to enhance the adsorption capacity of PG [20,25]. Under various incinerating temperatures, multifarious water situated in intracrystal channels of PG could be selectively evaporated and the pore structure, surface properties, and the SSA would be consequentially altered [25]. Gan et al. (2009) obtained the maximum phosphate sorption capacity of 42 mg/g when PG was heated at 700 °C and suggested that the layers of the PG collapsed; the structure was folded and pores were blocked when PG was heated above 700 °C [26]. Additionally, it has been reported that cations, especially metal (hydr)oxide, lead to a positive surface charge of the adsorbent and enhance the effective adsorption sites for anions, which benefits phosphate adsorption [23,27,28]. Our previous study certificated that phosphate had a relatively strong affinity for the surface of PG and the coating of aluminum (hydr)oxide on PG contributed to the maximum phosphorus adsorptive density of 16.86 mg/g, while the value of natural PG was 4.08 mg/g [21]. Zhang et al. (2022) prepared La–Mg-modified PG composite for phosphate adsorption and found that metal-bound hydroxyl and metal oxide groups dedicated great efforts on a high adsorptive quantity of 104.22 mg P/g [2]. Wang et al. (2017) prepared PG–MgO to adsorb phosphate from aqueous solution and found the loading of MgO extremely magnified the maximum phosphorus sorption density from 1.49 (raw PG) to 69.8 mg/g (PG–MgO) [29]. To enhance the application and fulfill the purpose of phosphorus recovering, a recyclable and easily dissociated adsorbent is desired. Many studies verified that  $\text{Fe}_3\text{O}_4$  can achieve these requirements [12,16,30–32]. Magnetic-based materials have greater surface area, higher adsorption capacity, low cost, intensified stability, and magnetic separation properties [30,33]. Jack et al. (2019) fabricated magnetic biochar to adsorb phosphate and received a maximum adsorptive density of 23.9 mg/g [12]. Wang et al. (2021) compared raw diatomite and magnetic  $\text{Fe}^0$ /iron oxide-coated diatomite on phosphorus adsorption and found the adsorptive densities were 3.51 and 37.0 mg P/g, respectively [32]. However, few studies have been conducted to remove phosphorus using magnetic thermal modified PG (MTPG) as an adsorbent.

Here, MTPG was firstly fabricated and systematically evaluated the feasibility of its application on the phosphate adsorption from aquatic medium. In doing this, the impact of pH, ionic strength, and regeneration cycles were evaluated by batch experiments. Values from well-known adsorption isotherms, thermodynamic parameters, and kinetic models were applied to explore the mechanism of condensed phosphate binding to the surface of MTPG.

## 2. Materials and Methods

### 2.1. Materials

The natural palygorskite (PG) mineral (<200 mesh) for modification was obtained from Guanshan, Anhui, China. The thermal modified palygorskite (TPG) was achieved by heat treatment at 700 °C in a muffle furnace for 2 h. The preparation method of MTPG followed a modification procedure reported by Mu et al. [16]. Firstly, 2 g FeCl<sub>3</sub>, 1.2 g polyethylene glycol, and 5.0 g sodium acetate were added into 60 mL ethylene glycol solution in sequence and then the mixture was stirred for 30 min; 2 g TPG was dispersed to the medium and continually ultrasonicated for 3 h. Afterwards, transferred to a polytetrafluoroethylene-lined autoclave (100 mL), the latter suspension was calcined at a temperature of 180 °C for 12 h. The black composite after cooling to ambient temperature was bathed by using ethanol and deionized water for a few times until the conductivity was below 10 µs/cm. The dry MTPG nanocomposite was obtained after drying at 50 °C for 24 h.

Except PG, other chemicals employed in the current contribution were analytical reagents.

### 2.2. Batch Adsorption Experiments

The impact of pH and ion strength on the adsorptive capacity of phosphate onto MTPG was conducted under ambient temperature. In a series of 100 mL polyethylene centrifuge tubes with caps, PO<sub>4</sub><sup>3-</sup>-P solutions (50 mL, 1000 mg/L) were respectively regulated at different NaClO<sub>4</sub> concentrations of 0.001, 0.01, and 0.1 M and different pH values of 3, 4, 5, 6, 7, 8, 9, and 10 by 0.1–1M HClO<sub>4</sub> or 0.1–1M NaOH solutions. A total mass of 0.02 g MTPG was respectively mixed into the phosphate solution. The mixture was then mingled using a thermostatic shaker at a temperature of 25 °C for 12 h (250 rpm). After equilibrium, the solid phase was completely separated from the mixture by magnetic attraction, centrifuge, or membrane filter (0.45 µm). The PO<sub>4</sub><sup>3-</sup>-P concentration in liquid phase was examined.

The study of adsorption isotherms of phosphate was conducted in a thermostatic shaker for 24 h and the temperatures were set at 298 K, 308 K, and 318 K. A total mass of 0.02 g MTPG was mixed into the PO<sub>4</sub><sup>3-</sup>-P solutions (50 mL) at pH of 5 and initial PO<sub>4</sub><sup>3-</sup>-P concentrations of 5, 50, 100, 200, 500, and 1000 mg/L.

The kinetic adsorption of phosphate was evaluated at pH value of 5 and at a temperature of 298 K. A total mass of 0.02g MTPG was added into the PO<sub>4</sub><sup>3-</sup>-P solutions (50 mL, 1000 mg/L). Samples were taken at a continuous interval of 0.25, 0.5, 1, 2, 4, 8, 12, and 24 h.

The influence of regeneration cycles on phosphate adsorption capacity was evaluated at pH of 5 and at a temperature of 298 K. The adsorbent (MTPG) after saturated adsorption was collected and then mixed with 250 mL NaOH solution (0.3 M) under stirring for 6 h. After that, the adsorbent (MTPG) was gathered and bathed with deionized water for several times. Finally, the regenerated MTPG was dried at 50 °C in an oven for 24 h and reused to adsorb phosphate from aqueous solution.

### 2.3. Analysis Methods

The PO<sub>4</sub><sup>3-</sup>-P concentration was detected by the molybdenum-blue ascorbic acid method with a spectrophotometer (722E, Spectrum Co., Shanghai, China). The analysis of mineral phases was undertaken by X-ray diffraction (XRD) analysis by an X-ray diffraction meter (SmartLab, Rigaku, Japan) with a Cu-target and a range of 5–70° at a scan rate of 10° min<sup>-1</sup>. The studies of morphology and nanostructures of mineral materials were carried out by a field emission scanning electron microscope (FESEM, Sigma 300, Zeiss Ltd., Cambridge, UK) with an electron acceleration voltage of 10 kV. The analysis of SSA and pore circumstances of materials were carried out by a surface area and pore size analyzer (Quanta NOVA 3000e, Quantachrome, Shanghai, China).

## 3. Results and Discussion

### 3.1. Characterization of Adsorbents

The XRD images of three materials (PG, TPG, and MTPG) are illustrated in Figure 1a. The characteristic diffraction peaks of natural PG were emerged at 2θ = 8.40, 13.86, 16.42,

19.90, 21.34, 23.06, and 35.34°, which agreed with a standard card (31-783) in the JCPDS (Joint Committee on Powder Diffraction Standards) [14]. The reflections at  $2\theta = 20.86, 27.34,$  and  $50.14^\circ$  were considered to be quartz (JCPDS 85-795). Dolomite (JCPDS 75-1656) as a paragenous mineral coexisting with PG was found at  $2\theta = 30.96^\circ$  in the pattern [34]. The diffraction peak of PG suddenly disappeared after thermal modification at 700 °C. It was attributed to the loss of coordination water, and adsorbed water of PG led to the change of channel dimensions [26], while the crystalline quartz remains virtually the same. The diffraction patterns at  $2\theta = 30.12, 35.54, 57.18,$  and  $62.72^\circ$  were authenticated as magnetite (JCPDS 19-629) in the sample of MTPG [33].

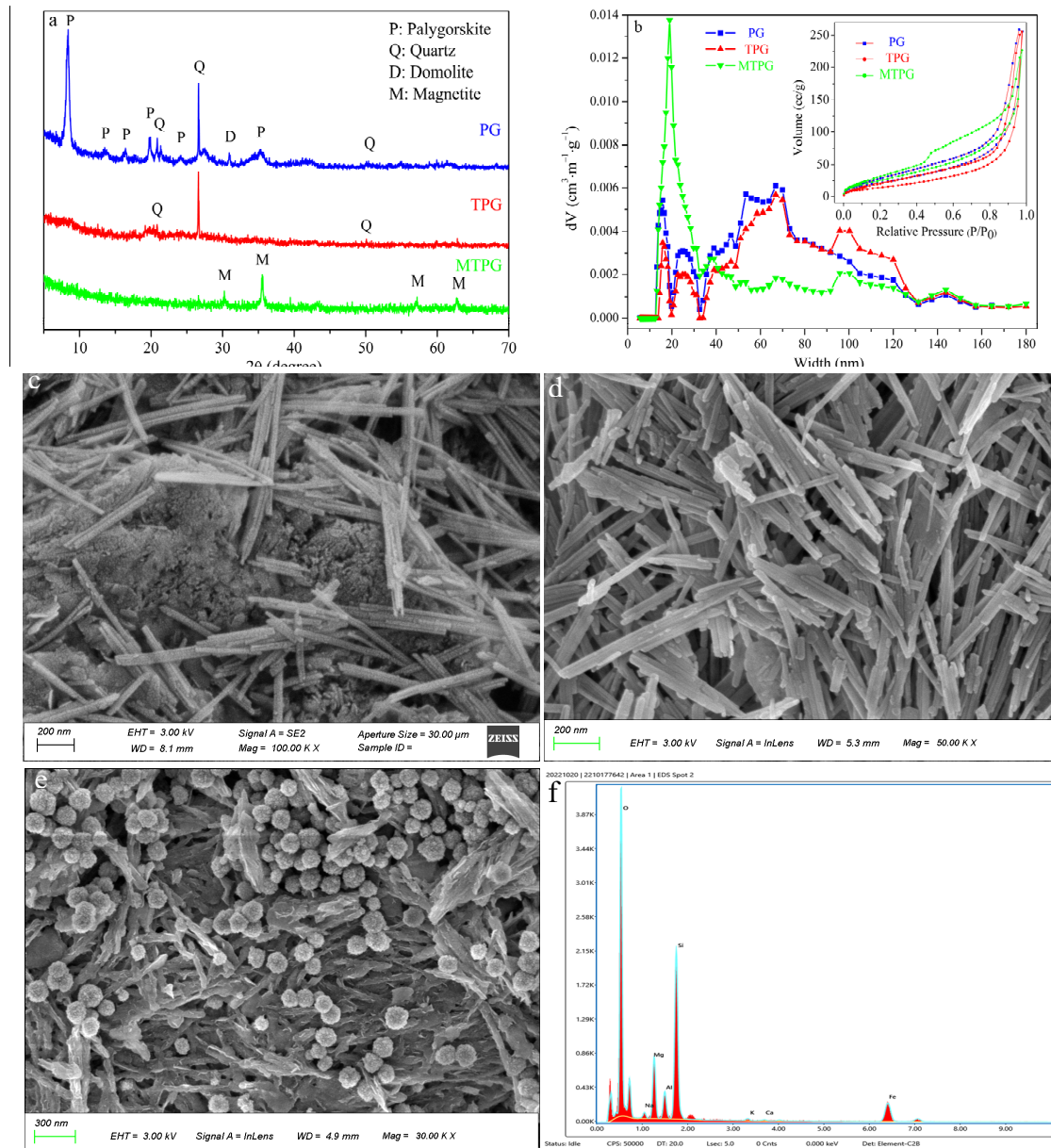


**Figure 1.** Characterization of mineral materials. (a) XRD patterns, (b) Pore size distributions and N<sub>2</sub>adsorption-desorption isotherms, (c) SEM of PG, (d) SEM of TPG, (e) SEM of MTPG, (f) EDS spectrum of MTPG.

The results of the BET-SSA and pore size distribution of PG, TPG, and MTPG are illustrated in Figure 1b. It can be observed that the adsorption/desorption curves were type IV isotherms, suggesting that the prepared samples were mineral materials with

mesoporous structure [35,36]. As seen in Figure 1b, the pore diameters of MTPG mainly in the range of 15–30 nm were smaller than that of PG and TPG. These mesoporous structures may dedicate higher SSA to magnify the adsorptive capacity [37]. The comparison of SSA, pore volume, and average pore size for PG, TPG, and MTPG is templated in Table 1. The SSA values of PG, TPG, and MTPG were 86.3, 57.0, and 104.7 m<sup>2</sup>/g, respectively. The SSA of TPG was decreased due to dehydration and dehydroxylation during the thermal treatment [26]. The value of synthesized MTPG composite was higher than that of TPG, which could be attributed by nanometer-sized Fe<sub>3</sub>O<sub>4</sub> [38].

**Table 1.** Specific surface area, average pore size, and pore volume of the materials.

Sample	BET-SSA (m <sup>2</sup> /g)	Average Pore Size (nm)	Pore Volume (cc/g)
PG	86.32	91.80	0.40
TPG	56.96	138.98	0.40
MTPG	104.72	66.90	0.35

The SEM images of PG, TPG, and MTPG used in the present study are shown in Figure 1c,d,f. Uniform nanorods with diameter of 20–30 nm and agglomerated nanocluster morphology of natural PG are displayed in Figure 1c. Particularly, the length of fibers was less than 2 μm. The room existing between the layers of TPG (Figure 1d) was declined because of the irreversible dehydration and dihydroxylation [26]. In addition, plenty of magnetite nanospheres (Figure 1e) with a scale of 100–200 nm were assembled on the glabrous surface of TPG after magnetic modification. The smaller size of magnetite comparing with previous work indicated that nano-scale PG improved the dispersion of magnetite particles and inhibited crystal growth [33,39]. The EDS analysis in Figure 1f further proved the loading of magnetite on TPG.

### 3.2. Effect of pH and Ionic Strength

The influence of pH on phosphate adsorption using MTPG as an adsorbent at pH arranging of 3–10 and different ionic strength is illustrated in Figure 2a. The sorption of phosphate onto MTPG is pH-dependent but slightly influenced by the ionic strength. The adsorptive density of phosphate was slightly magnified from 368.60 mg/g to 383.71 mg/g in the pH range of 3–6 and then sharply declined to 266.96 mg/g at pH of 10. It is reported that the adsorption of phosphate onto clay minerals is based on electrostatic attraction and ligand exchange [21]. According to the calculation results with visual MINTEQ, the primary species of phosphorus in liquids are H<sub>3</sub>PO<sub>4</sub> at pH < 2.15, H<sub>2</sub>PO<sub>4</sub><sup>−</sup> at pH 2.15–7.2, HPO<sub>4</sub><sup>2−</sup> at pH 7.2–12.3, and PO<sub>4</sub><sup>3−</sup> at pH > 12 (Figure 2b). The phosphate uptake capacities in acid condition are apparently greater than these in basic condition, which can be attributed to the bivalent HPO<sub>4</sub><sup>2−</sup> occupying more surface active sites of clay adsorbent than the monovalent H<sub>2</sub>PO<sub>4</sub><sup>−</sup> [40]. Additionally, electrostatic attraction benefited the positively charged active sites on MTPG appealed to phosphorus at lower pH [26]. Moreover, the p*H*<sub>pzc</sub> of MTPG was measured to be 6.8 in this research. When pH was lower than p*H*<sub>pzc</sub>, positively charged MTPG was benefited to unite negatively charged phosphate. A similar tendency had also been brought up in phosphorus sorption by natural PG [26,41], acid-modified PG [20,41], thermal treatment PG [26], and aluminum hydroxide-modified PG [21]. Moreover, the inner-spheric complexation was proved to be independent of ionic strength, while the outer-spheric complexation was uncontrollably affected by ionic strength [42]. Subsequently, one can infer that the adsorption behavior of phosphate on MTPG in the present study is predominant by the inner-spheric complexation [20].

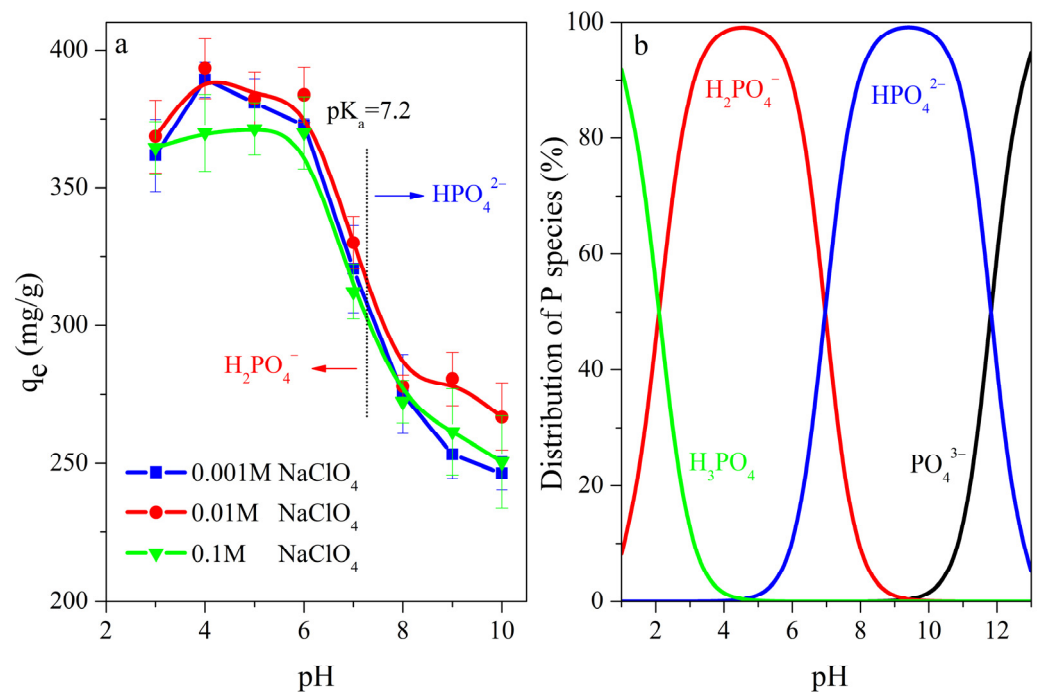


**Figure 2.** (a) Effect of initial pH on adsorption of phosphate on MTPG; (b) distribution of phosphorus species in liquids ( $C_0 = 1000$  mg/L, MTPG = 0.4 g/L,  $t = 12$  h,  $T = 298$  K).

### 3.3. Kinetics

In present study, there were three typical kinetic models employed to match the sorption kinetics of phosphate on MTPG, which are referred to as follows:

The equation of pseudo-first-order model [43]:

$$\ln(q_e - q_t) = \ln q_e - k_1 t \quad (1)$$

The equation of pseudo-second-order model [44]:

$$\frac{t}{q_t} = \frac{1}{k_2 q_e^2} + \frac{t}{q_e} \quad (2)$$

The equation of intraparticle diffusion model [45]:

$$q_t = k_3 t^{0.5} + C_{id} \quad (3)$$

where,  $q_e$  is the adsorbed capacity at equilibrium, mg/g;  $q_t$  is the adsorption amount at time  $t$ , mg/g;  $k_1$  is the rate constant of the pseudo-first-order adsorption,  $\text{h}^{-1}$ ;  $k_2$  is the rate constant of the pseudo-second-order adsorption,  $\text{g}/(\text{mg}\cdot\text{h})$ ;  $k_3$  is the intraparticle diffusion rate constant,  $\text{mg}/(\text{g}\cdot\text{h}^{-0.5})$ .  $C_{id}$  refers to the Weber–Morris constant, related to the thickness of the boundary layer, mg/g.

Figure 3a displayed the sorption kinetics of phosphate onto MTPG. The adsorption capacity significantly was speeded in the first 2 h, reaching 66.82% of the maximum adsorption capacity, and then slowly rose in the following 22 h. This performance may be prospectively interpreted by two reasons: (1) all the active sites on the surface of MTPG were available for phosphate adsorption at the beginning [2]; (2) along with the amount of active sites reducing and most of the surface area occupied by phosphate, the speeding of phosphate binding at the remaining active sites would be decelerated. The relevant parameters obtained here were all tabulated in Table 2. Comparing the correlation coefficients of three kinetic models, the highest  $R^2$  values obviously unveiled that the pseudo-second-order model best fit the adsorptive kinetics of phosphate on MTPG. The result obtained here was corresponding to other researches that the pseudo-second-order model successfully

simulated the kinetics sorption process of phosphate by PG [21,26], aluminum (hydr)oxide on PG [21], La–Mg-modified PG [2], acid-modified PG [20], thermally treated PG [26], ZrO<sub>2</sub>-zeolite [9], biochar [46], magnetic reed [30], magnetic iron oxide nanoparticles [47], and activated carbon loaded with Fe(III) oxide [48]. According to the intraparticle diffusion model, (i) the intraparticle diffusion involved in the process of phosphate adsorption causes the fitting plot to be linear; (ii) if these lines pass through the origin point, the intraparticle diffusion would be the rate-limiting step, and (iii) two or more slopes would be taking place in a multi-step sorption process [21,49]. The sorption behavior of phosphate onto MTPG covers two steps with a multilinearity (Figure 3b). If the value of  $C_{id}$  was not zero, it was considered that the sorption process was not uniquely controlled by the intraparticle diffusion [31]. Tao et al. (2022) reported that the bigger the  $C_{id}$  value represented the greater the influence of boundary layer [9]. Thus, it was reasonable to infer that the adsorption process of phosphate onto MTPG was principally controlled by the intraparticle diffusion and boundary layer diffusion.

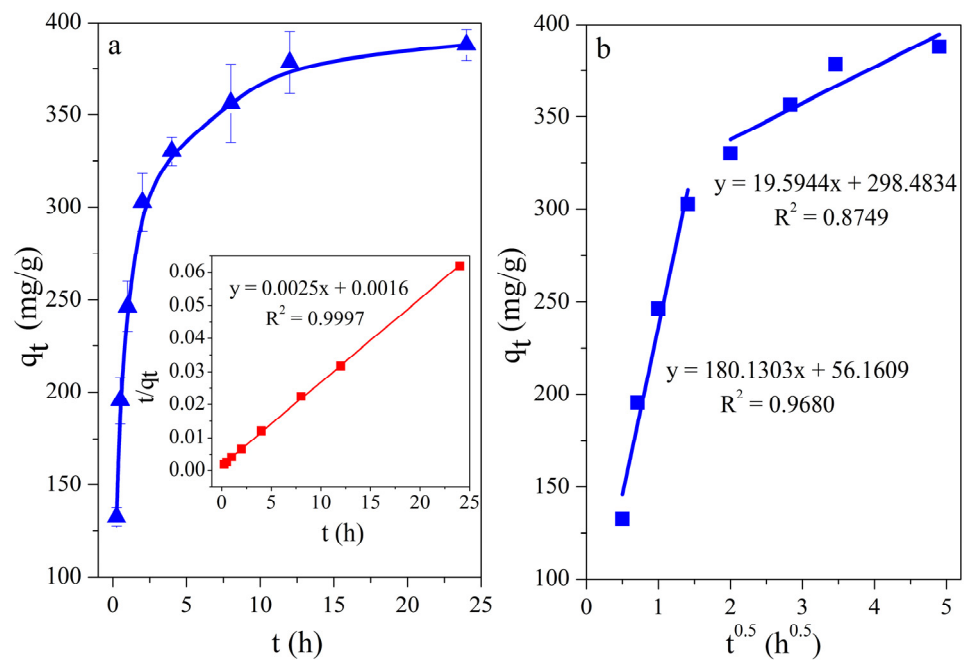


**Figure 3.** (a) Kinetics of phosphate sorption on MTPG and the pseudo-second-order fitting curve; (b) the intraparticle diffusion fitting curves ( $C_0 = 1000$  mg/L, MTPG = 0.4 g/L, pH = 5, T = 298 K).

**Table 2.** Kinetic parameters of phosphate sorption on MTPG.

Kinetic Models	Pseudo-First-Order			Pseudo-Second-Order			Intraparticle Diffusion					
	$q_e$ (mg/g)	$k_1$ (h <sup>-1</sup> )	$R^2$	$q_e$ (mg/g)	$k_2$ (g/mg·h)	$R^2$	$k_3$ (mg/g·h <sup>0.5</sup> )	$C_{id3}$ (mg/g)	$R^2$	$k_4$ (mg/g·h <sup>0.5</sup> )	$C_{id4}$ (mg/g)	$R^2$
MTPG	195.70	0.25	0.9597	400.00	0.0039	0.9997	180.13	56.16	0.9680	19.59	298.48	0.8749

### 3.4. Isotherms

The isotherms of phosphate sorption behavior on MTPG here were described by the Langmuir model [50], the Freundlich model [51], and the D-R isotherm [52]. The Langmuir model is expressed by the following Equation (4):

$$\frac{C_e}{q_e} = \frac{1}{q_m} C_e + \frac{1}{q_m k} \tag{4}$$

where  $C_e$  is the phosphate concentration at the equilibrium condition (mg/L);  $q_m$  is the maximum adsorptive capacity (mg/g);  $k$  is the Langmuir constant (L/mg).

The Freundlich model is given as Equation (5):

$$\ln q_e = \ln K_f + \frac{1}{n} \ln C_e \quad (5)$$

where,  $K_f$  is the Freundlich constant (mg/g);  $1/n$  refers to a heterogeneous factor, which represents the adsorption intensity or surface heterogeneity.

The D-R isotherm is represented as Equation (6):

$$\ln q_e = \ln q_m - \beta \varepsilon^2 \quad (6)$$

where  $\beta$  refers to the adsorptive energy constant ( $\text{mol}^2/\text{J}^2$ );  $\varepsilon$  represents Polanyi potential, which can be expressed as Equation (7):

$$\varepsilon = RT \ln\left(1 + \frac{1}{C_e}\right) \quad (7)$$

and  $E$  is the average adsorption energy (kJ/mol), which can be calculated from  $\beta$  as following:

$$E = \frac{1}{\sqrt{2\beta}} \quad (8)$$

The isotherms of phosphate adsorption onto MTPG are displayed in Figure 4a. The phosphate adsorption capacities were slightly increased with the increasing temperature and the adsorption was an endothermic process. Table 3 exhibits relevant parameters calculated from the adsorptive isotherm models under three different temperatures. Due to the values of  $R^2$  being bigger than 0.9, the Langmuir, Freundlich, and D-R isotherm can all be used to fit the adsorptive isotherm of phosphate onto MTPG. However, the Freundlich model gave the highest values of  $R^2$  ( $>0.9979$ ), which suggested that the adsorption occurred on the surface of a structurally heterogeneous adsorbent with exponentially decaying energies of adsorption sites [3]. In this study, the values of  $1/n$  calculated were between 0.4118 and 0.4340 ( $<0.5$ ), illustrating that the adsorption process of phosphate onto MTPG was favorable [3,32]. It also suggested the heterogeneous surface of MTPG and the multi-layer coverage of phosphate [3]. Moreover, the highest adsorptive quantity of 400 mg/g was counted according to the Langmuir model at 298 K. Table 4 templates the maximum phosphate adsorption capacities found in literature. Gan et al. (2009) mentioned that PG fulfilled dehydration over a temperature space of 80–540 °C and dehydroxylation over a temperature space of 540–770 °C, then Al and Fe in the PG would be activated and exposed at the surface of PG [26]. Thus, MTPG had plentiful active sites of Al, Fe, and  $\text{Fe}_3\text{O}_4$ , which all own great affinities for phosphate anions. Moreover, Hou et al. (2020) reported that nano-sized magnetite ( $n\text{Fe}_3\text{O}_4$ ) has a high surface area, large pore volume, high amounts of surface functional groups, and a low point of zero charge [53]. According to the D-R isotherm, the adsorption process of phosphate onto MTPG could be related to a pore volume filling process [52]. The  $E$  value differentiates the class of sorption, in which the values over the interval of 1–8 kJ/mol are on behalf of physical adsorption and of 8–16 kJ/mol symbolize chemical adsorption [54]. The points of  $E$  gained in the present study were in the range of 10.91–11.79 kJ/mol, verifying that the phosphate adsorption onto MTPG was predominantly chemisorption.

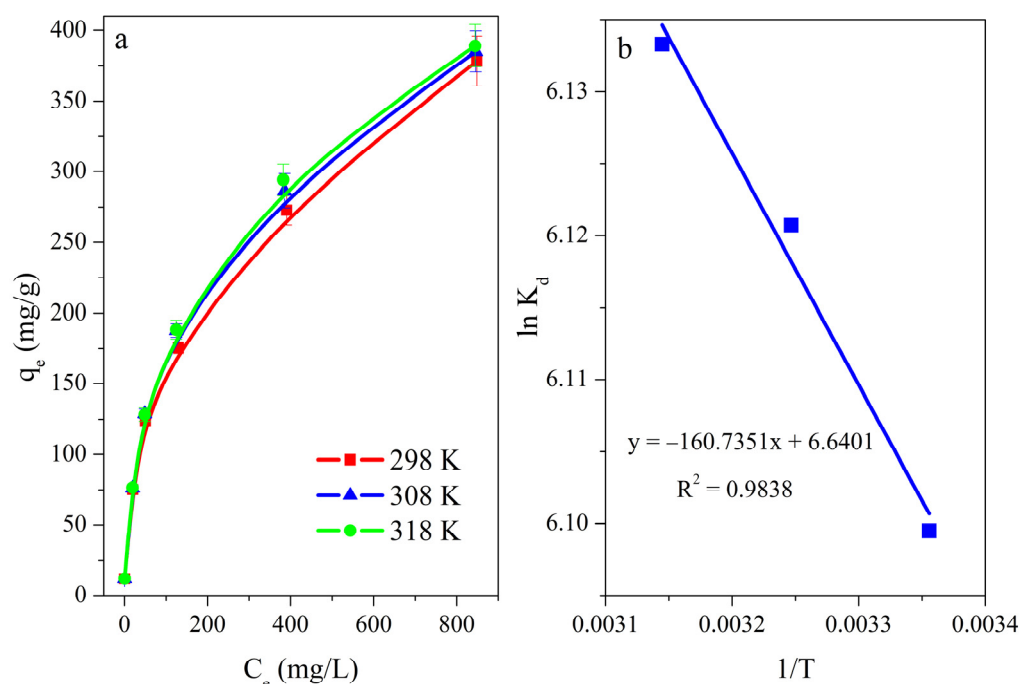


**Figure 4.** (a) Adsorption isotherms of phosphate on MTPG; (b) plots of  $\ln K_d$  vs.  $1/T$ . ( $C_0 = 5\text{--}1000$  mg/L, MTPG = 0.4 g/L, pH = 5, t = 24 h).

**Table 3.** Relative parameters of sorption isotherms models.

T (K)	Langmuir			Freundlich			D-R			
	$q_m$ (mg/g)	k (L/mg)	$R^2$	$K_f$ (mg/g)	1/n	$R^2$	$\beta$ (mol <sup>2</sup> /J <sup>2</sup> )	$q_m$ (mg/g)	E (kJ/mol)	$R^2$
298	400.00	0.0099	0.9595	23.48	0.41	0.9991	0.0041	400.52	11.04	0.9715
308	416.67	0.0104	0.9696	21.96	0.43	0.9979	0.0042	446.29	10.91	0.9802
318	416.67	0.0106	0.9703	24.31	0.42	0.9985	0.0036	425.16	11.79	0.9719

**Table 4.** The maximum phosphorus adsorption capacities reported in literature.

Adsorbent	Reaction Condition	Adsorption Capacity (mg/g)	Reference
Natural palygorskite	Adsorbent dosage: 0.5 g; initial P concentration: 5~1000 mg/L; pH = 4.46	10.9	Gan 2009 [26]
Thermally treated natural palygorskite	Adsorbent dosage: 0.5 g; initial P concentration: 5~1000 mg/L; pH = 4.46	42.0	Gan 2009 [26]
Hydroxy-iron-aluminum pillared bentonites	Adsorbent dosage: 4 g; initial P concentration: 20~60 mg/L; pH = 3	10.5	Yan 2010 [40]
Layered double hydroxide (LDH)-coated attapulgite	Adsorbent dosage: 0.1 g; initial P concentration: 2.5~200 mg/L	6.9	Gan 2011 [11]
Granular palygorskite	Adsorbent dosage: 0.5 g; initial P concentration: 5~1000 mg/L; pH = 6.86	13.1	Gan 2011 [55]
Acid-activated neutralized red mud	Adsorbent dosage: 0.5 g; initial P concentration: 50~1000 mg/L; pH = 4.5	396.35	Ye 2015 [13]
Zirconium (IV)-loaded cross-linked chitosan particles	Adsorbent dosage: 0.1 g; initial P concentration: 50~200 mg/L; pH = 3, 5, and 7	71.68	Liu 2016 [56]
Zirconium hydroxide modified by dimethylamine	Adsorbent dosage: 0.05 g; initial P concentration: 20~350 mg/L; pH = 6	155.04	Luo 2017 [57]

Table 4. Cont.

Adsorbent	Reaction Condition	Adsorption Capacity (mg/g)	Reference
Aluminum hydroxide-modified palygorskite nano-composites	Adsorbent dosage: 0.5 g; initial P concentration: 5~1000 mg/L; pH = 5	16.86	Pan 2017 [21]
Calcined nano-porous palygorskite matrix with embedded lanthanum hydroxide	Adsorbent dosage: 0.2 g; initial P concentration: 5~1000 mg/L; pH = 6.5~7	109.63	Kong 2018 [23]
La-Mg-modified palygorskite	Adsorbent dosage: 2 g; initial P concentration: 5~1000 mg/L; pH = 7	109.35	Zhang 2022 [2]
Magnetic thermal modified palygorskite	Adsorbent dosage: 0.02 g; initial P concentration: 5~1000 mg/L; pH = 5	400.00	The present study

### 3.5. Thermodynamic Parameters

In terms of temperature-dependent sorption isotherms, the thermodynamic parameters of phosphate adsorption in the present study can be calculated from the following Equations (9)–(11):

$$K_d = q_e / C_e \quad (9)$$

$$\Delta G^0 = -RT \ln K_d \quad (10)$$

$$\ln K_d = -\frac{\Delta H^0}{RT} + \frac{\Delta S^0}{R} \quad (11)$$

Here,  $K_d$  presents the distribution coefficient, ml/g;  $\Delta G^0$  (kJ/mol),  $\Delta H^0$  (kJ/mol), and  $\Delta S^0$  (J/mol) which are on behalf of the change of Gibbs energy, enthalpy, and entropy, respectively.

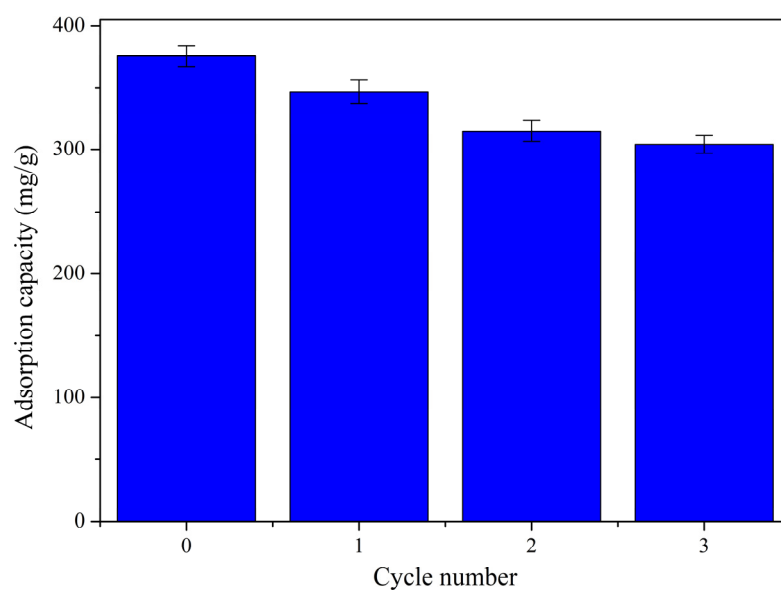
Figure 4b shows the plot of  $\ln K_d$  versus  $1/T$ . The slope of the line determines the change of  $\Delta H^0$ , while the intercept certifies the change of  $\Delta S^0$ . Table 5 shows the summary of  $\Delta G^0$ ,  $\Delta H^0$ , and  $\Delta S^0$  values. Negative  $\Delta G^0$  and positive  $\Delta H^0$  symbolized the adsorption behavior of phosphate onto MTPG as endothermic, feasible, and spontaneous [2]. The absolute data of  $\Delta G^0$  are positively correlated with the temperature. Thus, in the present study, the increasing of temperature magnified the spontaneous tendency of phosphate sorption onto MTPG. In particular, the positive value of  $\Delta S^0$  manifested the randomness or disorder increased at the solid–liquid interface in the process of phosphate binding to MTPG [9].

Table 5. Thermodynamic parameters of phosphate sorption on MTPG.

T(K)	$\Delta G^0$ (kJ/mol)	$\Delta S^0$ (kJ/mol/K)	$\Delta H^0$ (kJ/mol)
298	−15.112		
308	−15.673	0.055	1.336
318	−16.216		

### 3.6. Regeneration

For economic reasons, the exhausted adsorbent is required to be reused by a practical regeneration method [55]. The adsorption of phosphate onto MTPG was basically decayed at higher pH, thus sodium hydroxide solution may be efficient to phosphate desorption from the saturated adsorbent [31]. The regeneration of MTPG which went through the circle of regeneration is unveiled in Figure 5. It is apparently seen that the phosphate adsorption density gradually declines with a rise of the cycle sequence. After the third regeneration cycle, the adsorptive quantities in Figure 5 were obviously reduced from 375.46 mg/g to 304.05 mg/g, with the regeneration ratio of 80.98%. This finding proved that after regeneration, the reusability of MTPG was still feasible [31]. In particular, the MTPG was confirmed to possess great advantages on magnetic recovery and reused characteristics by employing a rapid sodium hydroxide regeneration method.



**Figure 5.** Reuse and regeneration of MTPG for phosphate uptake ( $C_0 = 1000$  mg/L, MTPG = 0.4 g/L, pH = 5,  $t = 24$  h).

#### 4. Conclusions

The MTPG with brilliant characteristics of magnetic recovery power was successfully fabricated in the present study. MTPG showed a great capability of phosphate adsorption from liquid solution. The isotherm model of Freundlich and the kinetic model of the pseudo-second-order satisfactorily fitted the adsorption process of phosphate onto MTPG. The maximum sorption quantity of 400 mg/g was achieved. The  $E$  values from the D-R isotherm in the range of 10.91–11.79 kJ/mol proved that the adsorption was chemisorption. The adsorptive process was verified by the thermodynamic parameters to be endothermic, feasible, and spontaneous. The adsorption process was inner-spherical complexation and governed by the intraparticle diffusion and boundary layer diffusion. By sodium hydroxide regeneration method, the regeneration ratio of 80.98% was obtained after the third regeneration cycle. The brilliant phosphate adsorption characteristics and magnetic recovery performance symbolized that MTPG can be a promising adsorbent extensively utilized in phosphate removal from aqueous solution.

**Author Contributions:** M.P.: writing, editing, supervision and funding acquisition. J.S., L.T. and Z.H.: investigation and methodology. X.H.: conception, design, investigation, writing, editing, and funding acquisition. All authors have read and agreed to the published version of the manuscript.

**Funding:** This research was funded by the Natural Science Foundation of Fujian Province (2021J011177, 2022J011231), the Innovation Project of College Students (S202111062023), and the Science and Technology Project of Longyan City (2017LY63).

**Acknowledgments:** The authors would like to acknowledge Shiyanjia Lab ([www.shiyanjia.com](http://www.shiyanjia.com), accessed on 17 October 2022) for the SEM-EDS analysis.

**Conflicts of Interest:** There are no conflict of interest to declare.

#### References

1. WHO Guidelines for Drinking Water Quality; World Health Organization: Geneva, Switzerland, 1993.
2. Zhang, C.; Wang, X.; Wang, X.; Liu, B. Characterization of La–Mg-modified palygorskite and its adsorption of phosphate. *J. Environ. Chem. Eng.* **2022**, *10*, 107658. [[CrossRef](#)]
3. Wang, B.; Hu, X.; Zhou, D.; Zhang, H.; Chen, R.; Guo, W.; Wang, H.; Zhang, W.; Hong, Z.; Lyu, W. Highly selective and sustainable clean-up of phosphate from aqueous phase by eco-friendly lanthanum cross-linked polyvinyl alcohol/alginate/palygorskite composite hydrogel beads. *J. Clean. Prod.* **2021**, *298*, 126878. [[CrossRef](#)]
4. Pan, M.; Huang, X.; Wu, G.; Hu, Y.; Yang, Y.; Zhan, X. Performance of denitrifying phosphate removal via nitrite from slaughterhouse wastewater treatment at low temperature. *Water* **2017**, *9*, 818. [[CrossRef](#)]

5. Shiba, N.; Ntuli, F. Extraction and precipitation of phosphorus from sewage sludge. *Waste Manage.* **2017**, *60*, 191–200. [[CrossRef](#)] [[PubMed](#)]
6. Kim, K.; Kim, D.; Kim, T.; Kim, B.G.; Ko, D.; Lee, J.; Han, Y.; Jung, J.C.; Na, H.B. Synthesis of mesoporous lanthanum hydroxide with enhanced adsorption performance for phosphate removal. *RSC Adv.* **2019**, *9*, 15257–15264. [[CrossRef](#)]
7. Wei, Y.; Guo, K.; Wu, H.; Yuan, P.; Liu, D.; Du, P.; Chen, P.; Wei, L.; Chen, W. Highly regenerative and efficient adsorption of phosphate by restructuring natural palygorskite clay via alkaline activation and co-calcination. *Chem. Commun.* **2021**, *57*, 1639–1642. [[CrossRef](#)]
8. Okano, K.; Yamamoto, Y.; Takano, H.; Aketo, T.; Honda, K.; Ohtake, H. A simple technology for phosphorus recovery using acid-treated concrete sludge. *Sep. Purif. Technol.* **2016**, *165*, 173–178. [[CrossRef](#)]
9. Tao, Y.; Liu, S.; Dong, S.; Wang, C.; Qu, T.; Li, S.; Li, L.; Ma, Z. An in situ grown amorphous ZrO<sub>2</sub> layer on zeolite for enhanced phosphate adsorption. *RSC Adv.* **2022**, *12*, 16751–16762. [[CrossRef](#)]
10. Wu, B.; Wan, J.; Zhang, Y.; Pan, B.; Lo, I.M.C. Selective phosphate removal from water and wastewater using sorption: Process fundamentals and removal mechanisms. *Environ. Sci. Technol.* **2020**, *54*, 50–66. [[CrossRef](#)]
11. Gan, F.; Zou, J.; Wang, H.; Zhao, H. Layered double hydroxide (LDH)-coated attapulgite for phosphate removal from aqueous solution. *Water Sci. Technol.* **2011**, *64*, 2192–2198.
12. Jack, J.; Huggins, T.M.; Huang, Y.; Fang, Y.; Ren, Z.J. Production of magnetic biochar from waste-derived fungal biomass for phosphorus removal and recovery. *J. Clean. Prod.* **2019**, *224*, 100–106. [[CrossRef](#)]
13. Ye, J.; Cong, X.; Zhang, P.; Hoffmann, E.; Zeng, G.; Liu, Y.; Fang, W.; Wu, Y.; Zhang, H. Interaction between phosphate and acid-activated neutralized red mud during adsorption process. *Appl. Surf. Sci.* **2015**, *356*, 128–134. [[CrossRef](#)]
14. Wang, C.; Zou, X.; Liu, H.; Chen, T.; Suib, S.L.; Chen, D.; Xie, J.; Li, M.; Sun, F. A highly efficient catalyst of palygorskite-supported manganese oxide for formaldehyde oxidation at ambient and low temperature: Performance, mechanism and reaction kinetics. *Appl. Surf. Sci.* **2019**, *486*, 420–430. [[CrossRef](#)]
15. Pan, M.; Wang, N.; Weng, Z.; Zou, X.; Huang, X. The synergistic activation of peroxymonosulfate for the degradation of Acid Scarlet GR by palygorskite/MnO<sub>2</sub>/Fe<sub>3</sub>O<sub>4</sub> nanocomposites. *Dalton Trans.* **2023**, *52*, 1009–1020. [[CrossRef](#)]
16. Mu, B.; Wang, Q.; Wang, A. Preparation of magnetic attapulgite nanocomposite for the adsorption of Ag<sup>+</sup> and application for catalytic reduction of 4-nitrophenol. *J. Mater. Chem. A* **2013**, *1*, 7083. [[CrossRef](#)]
17. Zha, F.; Huang, W.; Wang, J.; Chang, Y.; Ding, J.; Ma, J. Kinetic and thermodynamic aspects of arsenate adsorption on aluminum oxide modified palygorskite nanocomposites. *Chem. Eng. J.* **2013**, *215–216*, 579–585. [[CrossRef](#)]
18. Yin, H.; Kong, M. Simultaneous removal of ammonium and phosphate from eutrophic waters using natural calcium-rich attapulgite-based versatile adsorbent. *Desalination* **2014**, *351*, 128–137. [[CrossRef](#)]
19. Qiu, G.; Xie, Q.; Liu, H.; Chen, T.; Xie, J.; Li, H. Removal of Cu(II) from aqueous solutions using dolomite–palygorskite clay: Performance and mechanisms. *Appl. Clay Sci.* **2015**, *118*, 107–115. [[CrossRef](#)]
20. Li, F.; Wu, W.; Li, R.; Fu, X. Adsorption of phosphate by acid-modified fly ash and palygorskite in aqueous solution: Experimental and modeling. *Appl. Clay Sci.* **2016**, *132–133*, 343–352. [[CrossRef](#)]
21. Pan, M.; Lin, X.; Xie, J.; Huang, X. Kinetic, equilibrium and thermodynamic studies for phosphate adsorption on aluminum hydroxide modified palygorskite nano-composites. *RSC Adv.* **2017**, *7*, 4492–4500. [[CrossRef](#)]
22. Wu, X.; Zhu, W.; Zhang, X.; Chen, T.; Frost, R. Catalytic deposition of nanocarbon onto palygorskite and its adsorption of phenol. *Appl. Clay Sci.* **2011**, *52*, 400–406. [[CrossRef](#)]
23. Kong, L.; Tian, Y.; Li, N.; Liu, Y.; Zhang, J.; Zuo, W. Highly-effective phosphate removal from aqueous solutions by calcined nano-porous palygorskite matrix with embedded lanthanum hydroxide. *Appl. Clay Sci.* **2018**, *162*, 507–517. [[CrossRef](#)]
24. Zhang, J.; Xie, S.; Ho, Y.-S. Removal of fluoride ions from aqueous solution using modified attapulgite as adsorbent. *J. Hazard. Mater.* **2009**, *165*, 218–222. [[CrossRef](#)] [[PubMed](#)]
25. Chen, H.; Zhao, J.; Zhong, A.; Jin, Y. Removal capacity and adsorption mechanism of heat-treated palygorskite clay for methylene blue. *Chem. Eng. J.* **2011**, *174*, 143–150. [[CrossRef](#)]
26. Gan, F.; Zhou, J.; Wang, H.; Du, C.; Chen, X. Removal of phosphate from aqueous solution by thermally treated natural palygorskite. *Water Res.* **2009**, *43*, 2907–2915. [[CrossRef](#)]
27. Hilbrandt, I.; Shemer, H.; Ruhl, A.S.; Semiat, R.; Jekel, M. Comparing fine particulate iron hydroxide adsorbents for the removal of phosphate in a hybrid adsorption/ultrafiltration system. *Sep. Purif. Technol.* **2019**, *221*, 23–28. [[CrossRef](#)]
28. Bouraie, M.E.; Masoud, A.A. Adsorption of phosphate ions from aqueous solution by modified bentonite with magnesium hydroxide Mg(OH)<sub>2</sub>. *Appl. Clay Sci.* **2017**, *140*, 157–164. [[CrossRef](#)]
29. Wang, H.; Wang, X.; Xia, P.; Song, J.; Ma, R.; Jing, H.; Zhang, Z.; Cheng, X.; Zhao, J. Eco-friendly synthesis of self-existed magnesium oxide supported nanorod-like palygorskite for enhanced and simultaneous recovery of nutrients from simulated wastewater through adsorption and in-situ struvite formation. *Appl. Clay Sci.* **2017**, *135*, 418–426. [[CrossRef](#)]
30. Wang, T.; Xu, X.; Ren, Z.; Gao, B.; Wang, H. Adsorption of phosphate on surface of magnetic reed: Characteristics, kinetic, isotherm, desorption, competitive and mechanistic studies. *RSC Adv.* **2016**, *6*, 5089–5099. [[CrossRef](#)]
31. Song, X.; Hao, Y.; Gao, Q.; Cheng, L. Preparation and performance of magnetic zirconium-iron oxide nanoparticles loaded on palygorskite in the adsorption of phosphate from water. *Química Nova* **2022**, *45*, 1214–1222. [[CrossRef](#)]
32. Wang, J.; Zhang, G.; Qiao, S.; Zhou, J. Magnetic Fe<sup>0</sup>/iron oxide-coated diatomite as a highly efficient adsorbent for recovering phosphorus from water. *Chem. Eng. J.* **2021**, *412*, 128696. [[CrossRef](#)]

33. Huang, X.; Wang, N.; Kang, Z.; Yang, X.; Pan, M. An investigation into the adsorption of ammonium by zeolite-magnetite composites. *Minerals* **2022**, *12*, 256. [[CrossRef](#)]
34. Xie, J.; Chen, T.; Xing, B.; Liu, H.; Xie, Q.; Li, H.; Wu, Y. The thermochemical activity of dolomite occurred in dolomite-palygorskite. *Appl. Clay Sci.* **2016**, *119*, 42–48. [[CrossRef](#)]
35. Huang, C.; Wang, Y.; Gong, M.; Wang, W.; Mu, Y.; Hu, Z.  $\alpha$ -MnO<sub>2</sub>/Palygorskite composite as an effective catalyst for heterogeneous activation of peroxymonosulfate (PMS) for the degradation of Rhodamine B. *Sep. Purif. Technol.* **2020**, *230*, 115877. [[CrossRef](#)]
36. Wang, Y.; Xie, Y.; Sun, H.; Xiao, J.; Cao, H.; Wang, S. 2D/2D nano-hybrids of gamma-MnO<sub>2</sub> on reduced graphene oxide for catalytic ozonation and coupling peroxymonosulfate activation. *J. Hazard. Mater.* **2016**, *301*, 56–64. [[CrossRef](#)]
37. Sousa, A.F.d.; Braga, T.P.; Gomes, E.C.C.; Valentini, A.; Longhinotti, E. Adsorption of phosphate using mesoporous spheres containing iron and aluminum oxide. *Chem. Eng. J.* **2012**, *210*, 143–149. [[CrossRef](#)]
38. Liu, Y.; Liu, P.; Su, Z.; Li, F.; Wen, F. Attapulgite-Fe<sub>3</sub>O<sub>4</sub> magnetic nanoparticles via co-precipitation technique. *Appl. Surf. Sci.* **2008**, *255*, 2020–2025. [[CrossRef](#)]
39. Yu, Y.; Ji, Y.; Lu, J.; Yin, X.; Zhou, Q. Degradation of sulfamethoxazole by Co<sub>3</sub>O<sub>4</sub>-palygorskite composites activated peroxymonosulfate oxidation. *Chem. Eng. J.* **2021**, *406*, 126759. [[CrossRef](#)]
40. Yan, L.G.; Xu, Y.Y.; Yu, H.Q.; Xin, X.D.; Wei, Q.; Du, B. Adsorption of phosphate from aqueous solution by hydroxy-aluminum, hydroxy-iron and hydroxy-iron-aluminum pillared bentonites. *J. Hazard. Mater.* **2010**, *179*, 244–250. [[CrossRef](#)]
41. Ye, H.; Chen, F.; Sheng, Y.; Sheng, G.; Fu, J. Adsorption of phosphate from aqueous solution onto modified palygorskites. *Sep. Purif. Technol.* **2006**, *50*, 283–290. [[CrossRef](#)]
42. Sun, Y.; Yang, S.; Sheng, G.; Guo, Z.; Tan, X.; Xu, J.; Wang, X. Comparison of U(VI) removal from contaminated groundwater by nanoporous alumina and non-nanoporous alumina. *Sep. Purif. Technol.* **2011**, *83*, 196–203. [[CrossRef](#)]
43. Lagergren, S. About the Theory of So-Called Adsorption of Soluble Substances. *Kung. Sven. Vetensk. Hand.* **1898**, *24*, 1–39.
44. Ho, Y.S.; McKay, G. Pseudo-second order model for sorption processes. *Process. Biochem.* **1999**, *34*, 451–465. [[CrossRef](#)]
45. McKay, G.; Poots, V.J.P. Kinetics and diffusion processes in colour removal from effluent using wood as an adsorbent. *J. Chem. Technol. Biotechnol.* **1980**, *30*, 279–292. [[CrossRef](#)]
46. Feng, Y.; Zhao, D.; Qiu, S.; He, Q.; Luo, Y.; Zhang, K.; Shen, S.; Wang, F. Adsorption of phosphate in aqueous phase by biochar prepared from sheep manure and modified by oyster shells. *ACS Omega* **2021**, *6*, 33046–33056. [[CrossRef](#)] [[PubMed](#)]
47. Yoon, S.Y.; Lee, C.G.; Park, J.A.; Kim, J.H.; Kim, S.B.; Lee, S.H.; Choi, J.W. Kinetic, equilibrium and thermodynamic studies for phosphate adsorption to magnetic iron oxide nanoparticles. *Chem. Eng. J.* **2014**, *236*, 341–347. [[CrossRef](#)]
48. Shi, Z.; Liu, F.; Yao, S. Adsorptive removal of phosphate from aqueous solutions using activated carbon loaded with Fe(III) oxide. *New Carbon Mater.* **2011**, *26*, 299–306. [[CrossRef](#)]
49. Zhang, L.; Jin, S.; Wang, Y.; Ji, J. Phosphate adsorption from aqueous solution by lanthanum-iron hydroxide loaded with expanded graphite. *Environ. Technol.* **2018**, *39*, 997–1006. [[CrossRef](#)]
50. Langmuir, I. The adsorption of gases on plane surfaces of glass, mica and platinum. *J. Am. Chem. Soc.* **1918**, *40*, 1361–1403. [[CrossRef](#)]
51. Freundlich, H.M.F. Over the adsorption in solution. *J. Phys. Chem.* **1906**, *57*, 385–470.
52. Hu, Q.; Zhang, Z. Application of Dubinin-Radushkevich isotherm model at the solid/solution interface: A theoretical analysis. *J. Mol. Liq.* **2019**, *277*, 646–648. [[CrossRef](#)]
53. Hou, L.; Liang, Q.; Wang, F. Mechanisms that control the adsorption-desorption behavior of phosphate on magnetite nanoparticles: The role of particle size and surface chemistry characteristics. *RSC Adv.* **2020**, *10*, 2378–2388. [[CrossRef](#)] [[PubMed](#)]
54. Pan, M.; Zhang, M.; Zou, X.; Zhao, X.; Deng, T.; Chen, T.; Huang, X. The investigation into the adsorption removal of ammonium by natural and modified zeolites: Kinetics, isotherms, and thermodynamics. *Water SA* **2019**, *45*, 648–656. [[CrossRef](#)]
55. Gan, F.; Zhou, J.; Wang, H.; Du, C.; Zhang, W.; Chen, X. Phosphate adsorption on granular palygorskite: Batch and column studies. *Water Environ. Res.* **2011**, *83*, 147–153.
56. Liu, Q.; Hu, P.; Wang, L.; Zhang, L.; Huang, R. Phosphate adsorption from aqueous solutions by Zirconium (IV) loaded cross-linked chitosan particles. *J. Taiwan Inst. Chem. Eng.* **2016**, *59*, 311–319. [[CrossRef](#)]
57. Luo, X.; Wu, X.; Reng, Z.; Min, X.; Xiao, X.; Luo, J. Enhancement of phosphate adsorption on zirconium hydroxide by ammonium modification. *Ind. Eng. Chem. Res.* **2017**, *56*, 9419–9428. [[CrossRef](#)]

**Disclaimer/Publisher’s Note:** The statements, opinions and data contained in all publications are solely those of the individual author(s) and contributor(s) and not of MDPI and/or the editor(s). MDPI and/or the editor(s) disclaim responsibility for any injury to people or property resulting from any ideas, methods, instructions or products referred to in the content.